Mott-Hubbard transition in infinite dimensions. II

M. J. Rozenberg, G. Kotliar, and X. Y. Zhang

Serin Physics Laboratory, Rutgers University, Piscataway, New Jersey 08854
(Received 19 July 1993; revised manuscript received 1 October 1993)

We discuss the Mott-Hubbard transition in light of the Hubbard model in infinite dimensions with special emphasis on the finite-temperature aspects of the problem. We demonstrate that the Mott transition at finite temperatures has a first-order character. We determine the region where metallic and insulating solutions coexist using second-order perturbation theory and we draw the phase diagram of the Hubbard model at half filling with a semicircular density of states. We discuss the lessons learned from the present treatment of the Hubbard model and the connection to other approximation schemes and to experiments on transition-metal oxides.

I. INTRODUCTION

The Mott transition, which is the metal-insulator transition induced by the electron-electron interactions in a periodic system, has been investigated theoretically and experimentally for many years.[1] Experimentally it seems to be realized in three-dimensional transition-metal oxides such as V_2O_3 and can be driven by varying the pressure, the temperature, and the composition.

From a theoretical point of view, several ideas have been put forward. Hubbard first introduced the notion of Hubbard bands, which are formed by the states describing propagating empty and doubly occupied sites. For large U these bands split, and as U is reduced there is a critical value of U where the two bands merge again.[2] This is the Hubbard picture of the metal-insulating transition.

Brinkman and Rice,[3] building on the work of Gutzwiller, started from the metallic phase which they described as a strongly renormalized Fermi liquid with a characteristic Fermi energy scale gradually collapsing as the transition is approached. The metal-insulator transition in this view is driven by the disappearance of the Fermi liquid quasiparticles. Slater[4] pointed out that the metal-insulator transition is always accompanied by long-range antiferromagnetic order, and viewed the doubling of the unit cell, which makes the band structure of the system that of a band insulator, as the driving force behind the metal-insulator transition.

Building on earlier ideas,[5-9] a mean-field theory of strongly correlated electron systems has been developed. It is based on a mapping of the models of strongly correlated electrons onto impurity models supplemented by a self-consistent condition.[10,11] This approach becomes exact in the limit of infinite dimensions[5] and can be investigated using a variety of techniques. In this paper, we complete our study of the Mott transition in the Hubbard model in large dimension, expanding on our previous publications.[12,13] In particular, we make comparisons of our solutions to experimental observations, and find good agreement considering the relative simplicity of the model. Related work on this problem has been carried out independently by other groups.[14-17]

The paper is organized as follows: In Sec. II, we start by briefly reviewing the general framework of Ref. 11 to present the set of self-consistent equations that describe the Hubbard model in infinite dimensions. We concentrate on the semicircular density of states which can be realized on a Bethe lattice, or other lattices having various amounts of magnetic frustration. The mean-field equations are functional equations that determine a Weiss field function G_0 and involve a self-energy functional of an Anderson impurity model $\Sigma_{imp}[G_0]$. Two realizations of the Hubbard model which share the same density of states but have very different magnetic properties are introduced later to shed light on the issue of magnetic ordering. We close the section with a discussion of the methods used to analyze this problem.

To study the mean-field equations we use a combination of exact methods such as quantum Monte Carlo (QMC) and analytic arguments exploiting the well-understood structure of the Anderson impurity model. We also rely on an approximate method which was proposed by Georges and Kotliar to extract low-temperature information. We stress that, while at high temperature this method[13] gives results in very good agreement with the quantum Monte Carlo, in principle is only an approximate scheme and we point out some of its limitations. The results obtained with this method are useful because they provide a concrete analytic realization of the functional $\Sigma_{imp}[G_0]$ defined in Sec. II, and illustrate in a simple example the important role played by the self-consistency condition.[9]

In Sec. III we describe the thermodynamics and present the finite-temperature phase diagram of the system. We study the dependence of the phase diagram on the degree of magnetic frustration. In frustrated lattices the phase diagram features a region bounded by two values of the interaction U_{c1} and U_{c2}, where a metallic and an insulating phase coexist. The actual transition takes place at an intermediate value U_c where the free energies of the two solutions cross. We demonstrate that, at finite T, $U_{c1} < U_c < U_{c2}$, and the metal-insulator transition is of the first order, like a liquid-gas transition. While the region of stability of the two phases is model dependent and will vary upon changing the den-

sity of states or adding more general interactions to the Hamiltonian, there are some general lessons that can be drawn by studying the disappearance of the metallic and the insulating solution. These are general scenarios for describing a strongly correlated metal and a Mott insulator.

In Sec. IV we discuss the destruction of the metallic solution. It has many features in common with the Brinkman-Rice scenario for the disappearance of the metal and is realized near a critical value of the interaction U_{c2}.

In Sec. V we analyze the disappearance of the insulating solution. We show that there is another critical point U_{c1} below which the insulating solution disappears. The existence of this point is related to Hubbard's early ideas.

Section VI is devoted to the study of the correlation functions. In particular, we address the question of how they behave as the transition takes place. We rely on a combination of analytical arguments and QMC simulations to discuss these points.

In Sec. VII, we make qualitative comparisons to existing experimental data, in V_2O_3[18] and in $La_{1-x}Sr_xTiO_3$.[19] The agreement leads us to believe that the Hubbard model and its extended version are at least qualitatively correct models for describing these systems. We conclude with some theoretical questions raised by our work.

II. THE SELF-CONSISTENT EQUATIONS

We briefly review the self-consistent equations which give the paramagnetic solution in large d, following the scheme of Ref. 9. The central object in this approach is a quantity G_0 which plays the role of the effective field in magnetic systems. G_0 is defined in an effective local action S obtained by integrating out all the degrees of freedom except for a single site 0,

$$S[G_{0\sigma}] = -\int\int d\tau d\tau' c_\sigma^\dagger G_{0\sigma}^{-1} c_\sigma$$
$$+ \int d\tau U(n_\uparrow - \tfrac{1}{2})(n_\downarrow - \tfrac{1}{2}). \qquad (1)$$

This action is identical to that of an Anderson impurity model with arbitrary hybridization. The self-consistent equations for the Weiss field G_0 are written in terms of an impurity self-energy $\Sigma_{\text{imp}}(G_0) = \langle c^\dagger c\rangle_{S(G_0)}^{-1} + G_0^{-1}$ and the lattice density of states $\rho(\epsilon) = \sum_k \delta(\epsilon_k - \epsilon)$,

$$[G_0^{-1} - \Sigma_{\text{imp}}(G_0)]^{-1} = \int \frac{\rho(\epsilon)d\epsilon}{i\omega - \epsilon - \Sigma_{\text{imp}}(G_0)}. \qquad (2)$$

The impurity self-energy evaluated at the self-consistent G_0 gives the self-energy of the Hubbard model in infinite dimensions.[9]

We use a semicircular density of states, $\rho(\epsilon) = \frac{2}{\pi D}\sqrt{1 - (\frac{\epsilon}{D})^2}$. The set of self-consistent equations then becomes:

$$G_0^{-1} = i\omega_n - t^2 G(i\omega_n), \quad G = -\langle c^\dagger c\rangle_{S(G_0)} \qquad (3)$$

$G(i\omega_n)$ being the *local* Green's function of the Hubbard model. The spin index has been removed. This density of states is realized in the Bethe lattice with coordination d, in the limit that d becomes infinite, and with Hubbard's hopping parameter equal to $\frac{t}{\sqrt{d}}$. In this case $t = D/2$. This lattice with nearest-neighbor hopping, if not frustrated, will strongly favor a Néel-ordered state at low temperatures.

The semicircular density of states is also realized in the fully frustrated model,[12,20]

$$H_{\text{FF}} = -t\sum_{i,j=1,d} \epsilon_{ij} c_{i\sigma}^\dagger c_{j\sigma} + U\sum_i n_{i\uparrow}n_{i\downarrow}. \qquad (4)$$

Summation over repeated spin indices is assumed. Here ϵ_{ij} are quenched, independently distributed, Gaussian random variables with zero mean and a variance $\langle \epsilon_{ij}^2\rangle = \frac{1}{d}$. This model has a semicircular density of states with a bandwidth equal to $2t$ and therefore shares the same *local* properties as the Bethe lattice, but of course is not expected to display Néel order at any finite temperature. Finally we can vary the degree of frustration by studying a two-sublattice version of the fully frustrated model (TSFFM). The Hamiltonian is given by:

$$H_{\text{TSFFM}} = -t_1 \sum_{i,j\in A\,\text{or}\,B} \epsilon_{ij} c_{i\sigma}^\dagger c_{j\sigma}$$
$$-t_2 \sum_{i\in A\,j\in B} \epsilon_{ij} c_{i\sigma}^\dagger c_{j\sigma} + U\sum_{i\in A\cup B} n_{i\uparrow}n_{i\downarrow}. \qquad (5)$$

This model interpolates between the fully frustrated lattice and the Bethe lattice in the antiferromagnetic phase while still sharing a semicircular local density of states. In this case $D = \frac{\sqrt{t_1^2+t_2^2}}{2}$. Notice that while the Hamiltonians (4) and (5) contain randomness, the single-particle properties are self-averaging. The single-particle Green's functions are the same for any typical realization of the random variables ϵ_{ij}.

As in our previous publications, we have studied the semicircular density of states instead of the Gaussian density of states which is realized in the large-dimension limit of a hypercubic lattice, because the latter has long tails which prevent the development of a true Hubbard gap. For a study of the hypercubic lattice see Refs. 14 and 15.

When antiferromagnetism sets in, the Weiss field depends on the sublattice and the spin. For a general bipartite lattice in the Néel phase $G_{A\sigma} = G_{B-\sigma}$ the equations were derived in Ref. 11. For the Bethe lattice, the equations are simplified to:

$$G_{0A\sigma}^{-1} = i\omega - t^2 G_{B\sigma}, \qquad (6)$$

$$G_{0B\sigma}^{-1} = i\omega - t^2 G_{A\sigma}, \qquad (7)$$

where A denotes one sublattice and B the other. The two impurity Green's functions G_A and G_B are evaluated independently, given $G_{0A\sigma}$ and $G_{0B\sigma}$ and the single-site action S defined at the beginning of this section.

Finally, in the two-sublattice fully frustrated model, which mimics an intermediate degree of frustration, the

mean-field equations in a phase where the A and B sublattices magnetize in opposite directions are given by

$$G_{0A\sigma}^{-1} = iw - t_1^2 G_{A\sigma} - t_2^2 G_{B\sigma}, \qquad (8)$$

$$G_{0B\sigma}^{-1} = iw - t_1^2 G_{B\sigma} - t_2^2 G_{A\sigma}. \qquad (9)$$

In a previous work[13] we have discussed the fact that the exact treatment of the problem by a quantum Monte Carlo solution of the impurity can be reproduced, remarkably well, by the second-order perturbative calculation proposed in Ref. 21. The perturbative calculation allows us to investigate the low-temperature behavior of the system, including $T = 0$, which is unattainable by the QMC approach. To second order in perturbation,

$$\Sigma[G_0](\tau) = -U^2 G_0^3(\tau). \qquad (10)$$

We can understand the success of this approximation for the following reasons. (1) It is good for weak couplings ($U \ll t$) by construction, since the expansion is around $U = 0$. As shown by Yamada and Yosida (YY),[21] it is able to produce not only the Abrikosov-Suhl resonance, but also the upper and lower incoherent bands as well. YY showed that the fourth-order correction is two orders of magnitude smaller than the second-order contribution for the range of the interaction where the metal-insulator transition occurs. (2) The atomic limit is exactly captured. When U is very large, and the system is deep in the insulating side, $G_0^{-1} \approx i\omega_n$, the nonmagnetic Hartree-Fock solution of the Green's function becomes exact,

$$G_L(i\omega) = \frac{1/2}{G_0^{-1}(i\omega_n) - U/2} + \frac{1/2}{G_0^{-1}(i\omega_n) + U/2}, \qquad (11)$$

and therefore the self-energy reads,

$$\Sigma = \left(\frac{U}{2}\right)^2 G_0(i\omega_n), \qquad (12)$$

which is identical to the self-energy that results from inserting G_0 in Eq. (10) and Fourier transforming. Thus, the second-order approximation is at least an interpolation scheme which becomes exact for both the $U \to 0$ and $U \to \infty$ limits.

III. PHASE DIAGRAM AND THERMODYNAMICS

As discussed in previous publications, the system of Eqs. (1), (2), and (3) has two types of solutions, metallic when $G(0) = \frac{2}{iD}$ and insulating when $G(0) = 0$. This distinction is precise at zero temperature. At finite but small temperatures, a sharp distinction between a metallic and an insulating solution can still be made, since we find a region where *two* solutions are allowed. One can be continuously connected to the $T = 0$ metallic solution, and displays a peaklike feature at the Fermi energy. The other solution can be connected to the $T = 0$ insulating solution, and the Green's function extrapolates to zero at zero frequency. As the temperature is further increased

this region of coexistent solutions disappears and we are left with a rapid crossover from a metalliclike solution to an insulating one. This is possible because at finite temperature there is no qualitative distinction between a metallic and an insulating shape.

As mentioned in the introduction, at low temperatures there are two critical values U_{c1} (the smallest U that allows an insulating solution) and U_{c2} (the largest U permitting a metallic solution) between which the mean-field equations have two solutions. To determine the phase diagram we proceed in three steps: (a) We first determine the region where the two paramagnetic solutions coexist. (b) We then compare their free energy, crossing of which determines the phase boundary. (c) We finally study the magnetically ordered phase and calculate the Néel temperature to check whether the metal-insulator transition found in step (b) is preempted by a magnetic ordering transition.

We use the second-order perturbation theory scheme throughout most of this work because the low temperature prevents the extensive use of QMC. We checked however that the existence of two solutions is a genuine feature of the large-d Hubbard model and not an artifact of the second-order approximation by performing a few quantum Monte Carlo runs. In Fig. 1 we show a metallic and an insulating Green's function obtained for the same value of the parameters U=2.8 and T=1/64, as is obtained from both QMC and the perturbative calculation. Throughout the paper the bandwidth D is taken to be unity. To select an insulating or a metallic solution we choose G_0 obeying $G_0(i\omega) = \frac{1}{i\omega}$ or $G_0(0) \neq 0$ respectively as the initial guess in the substitution procedure for solving the mean-field equations.

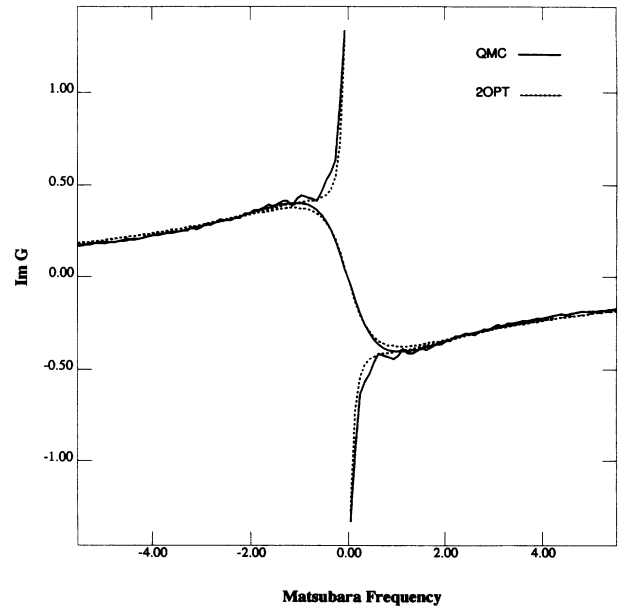The energy is computed from the Green's function by

FIG. 1. Comparison of the insulating and metallic Green's function obtained using the quantum Monte Carlo algorithm and the perturbative calculation. The value of the interaction $U = 2.8$ and the inverse temperature $\beta = 64$.

$$E = T\frac{1}{2}\sum_{nk}(i\omega_n + \epsilon_k)G_k(i\omega_n). \tag{13}$$

The entropy is given by

$$S(T) = \int_0^T \frac{C_v}{T'}dT' + S(0), \tag{14}$$

where C_v is evaluated numerically by differentiating the energy. $S(0)$ is zero for the metallic side and $\ln(2)$ for the insulating side, reflecting the double degeneracy of the paramagnetic insulating phase.

The physical critical line where the first-order phase transition takes place is determined by equating the free energies of the two states,

$$F_M - F_I = E_M - E_I - (S_M - S_I)T. \tag{15}$$

To gain insights into the nature of the two coexistent solutions we plot the zero-temperature spectral function of the metallic and the insulating state in Fig. 2. The metallic state of the system can be well described by a narrow central quasiparticle peak characterized by an effective Fermi energy $\Delta \equiv zD$ where z is the quasiparticle weight, $z = (1 - \frac{d\Sigma}{d\omega})^{-1}$, plus two high-energy incoherent features at $\pm\frac{U}{2}$ corresponding to the upper and lower Hubbard bands. The quasiparticle weight z as a function of U is shown in Fig. 3. The insulator state consists of incoherent features only. Notice however that the shapes of the incoherent features of the metallic and the insulating phase are very different.

Figure 4 shows the calculated internal energy as a function of the temperature for two values of the interaction U. For the smaller value of U the tempera-

FIG. 3. Quasiparticle weight z as a function of interaction U, obtained with the $T = 0$ self-consistent perturbative calculation.

ture dependence of the internal energy of the metal displays a characteristic Fermi liquid T^2 behavior in the low-temperature region. The characteristic energy scale in this regime is set by the renormalized Fermi energy. At higher temperatures we see a thermal activation of the incoherent features. In the case of the insulator we observe only this last effect at an energy scale $U - 2D$.

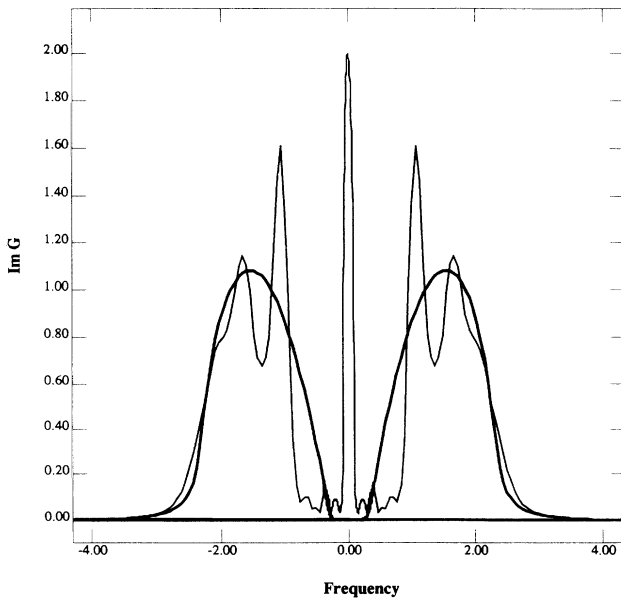In Fig. 5 we plot the specific heat C_v as a function

FIG. 2. Density of states for the metallic (thin line) and insulating (bold line) solutions at $T = 0$ and the same value of the interaction $U = 2.9$, obtained with the self-consistent perturbative calculation.
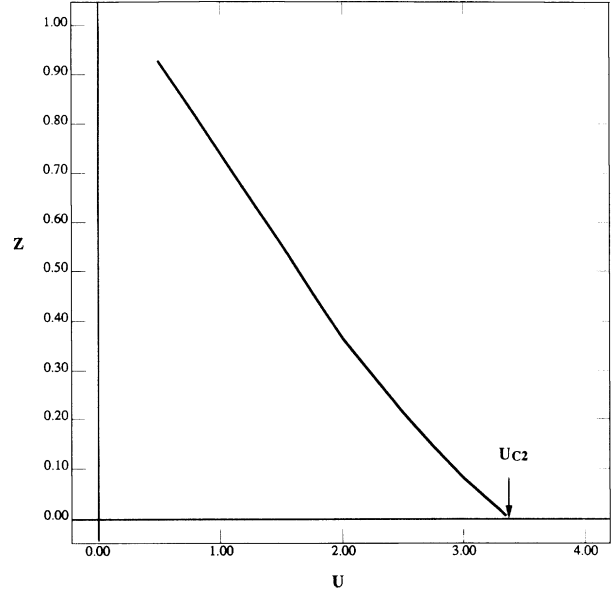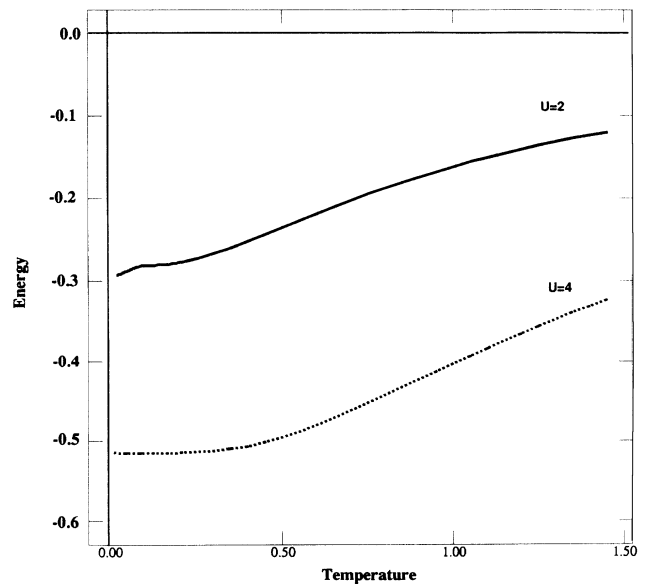

FIG. 4. Energy as a function of the temperature for a value of $U = 2$ in the metallic region (solid line), and $U = 4$ in the insulating phase (dotted line).
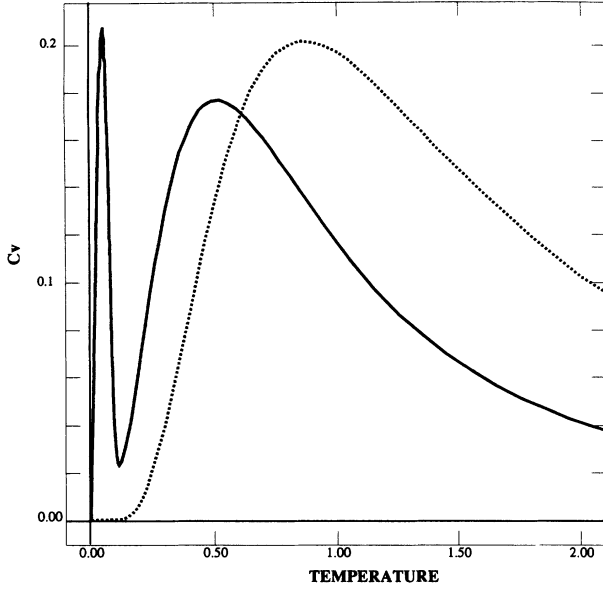
FIG. 5. Specific heat C_v as a function of temperature. The solid line is for $U = 2$ and the dashed line corresponds to $U = 4$. In the metallic case ($U = 2$) it is apparent the separation of energy scales. The linear part, at low T, ends at $T \sim \Delta$, and the thermal activation of the incoherent features peaks at the bigger scale $T \sim U - 2D$. This last effect is the only one present in the insulating case.

FIG. 6. Specific heat C_v as a function of temperature for several values of U.

of the temperature. The curves are obtained through numerical differentiation of $E(T)$. In the strongly correlated metallic phase we find a separation of scales since Δ is much smaller than $U - 2D$. At higher T a thermal activation peak appears at a scale $U - 2D$ in both the metallic and insulating cases. The linear-in-T Fermi liquid behavior is observed in the low-temperature region, with the slope γ proportional to $m^* \sim (U_{c2} - U)^{-1}$, as shown in Fig. 6

The integral (14) gives the entropy as a function of temperature. As expected the integral over the quasiparticle peak is equal to ln2 as shown in Fig. 7. As can be seen in Fig. 6, for larger values of U but with $U < U_{c2}$ the metallic solution disappears discontinuously before the entropy reaches ln2. Therefore, we define a coherence temperature T_s as the temperature where the entropy reaches the value of $\frac{\ln 2}{2}$. The physical relevance of T_s is that it delineates the temperature range where Fermi liquid theory is valid; see Fig. 8.

The comparison of the kinetic energy $T = \langle \sum_k \epsilon_k c_k^\dagger c_k \rangle = \sum_{nk} \epsilon_k G_k(i\omega_n)$ and the potential energy $V = U \sum \langle n_\uparrow n_\downarrow \rangle$ of the two solutions, is shown in Fig. 9 We find that the difference in the internal energy of the two states is much smaller than the corresponding difference in the kinetic and potential energy. The gain in kinetic energy by delocalization is almost perfectly canceled by the loss in potential energy due to the Coulomb repulsion in doubly occupied sites. This makes the higher-order corrections from higher-order terms in
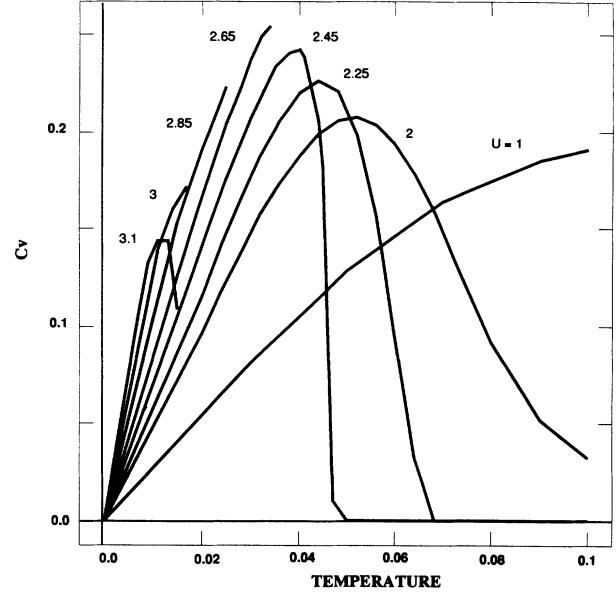
the Yamada-Yosida perturbation theory important for resolving the relative stability of the metallic and the insulating solution at zero temperature. We nevertheless expect the small energy difference between the two states to be a general feature of the problem and not an artifact of second-order perturbation theory. In fact the near degeneracy of the metallic and the insulating states near U_{c2} follows from the bifurcation of two stationary points of the free-energy functional at U_{c2}

We can take advantage of the numerical speed of the perturbative calculation to obtain a detailed phase diagram for the model defined by Eqs. (1), (2), and (3). The first-order phase boundary is determined by the crossing of the free energy of the two solutions. It ends in a crit-
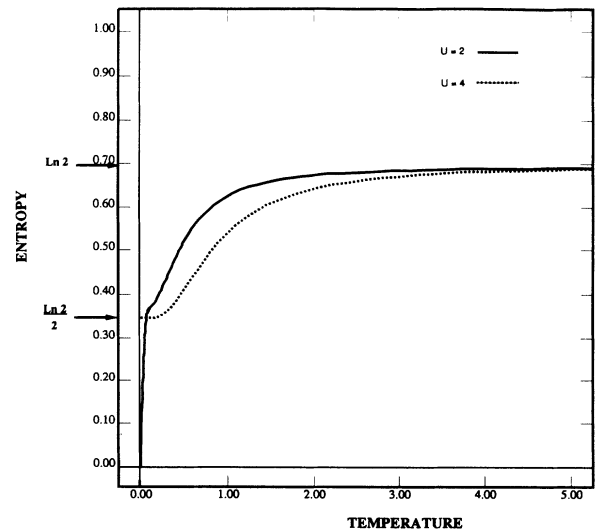

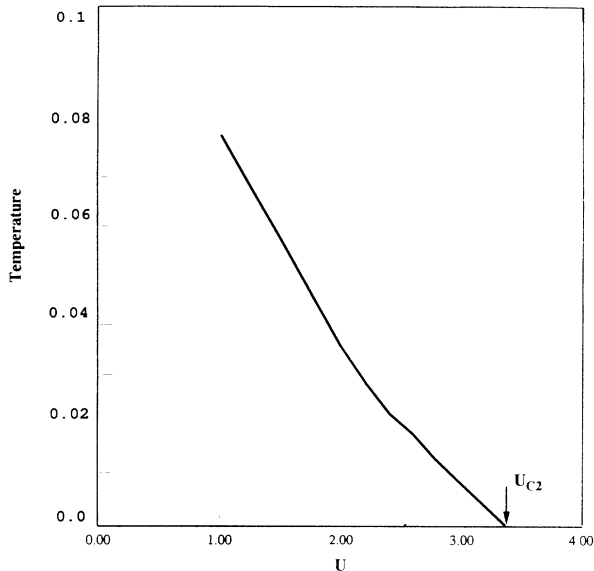FIG. 7. Entropy per spin as a function of temperature for two different values of interaction, $U = 2, 4$.

FIG. 8. Temperature value where the entropy reaches $\frac{\ln 2}{2}$ as a function of the distance to U_{c2}. This temperature defines the region where the Fermi liquid description is applicable.

ical point where a crossover region starts. This is displayed in Fig. 10. As emphasized before, due to the very small energy difference between the solutions, we expect the position of the phase boundary to be only approximately correct. We have observed in QMC runs that, for instance, the value of the U_{c1} line that denotes the disappearance of the insulating solution was shifted to a smaller value of the interaction U by an amount of order of $\sim 10\%$.
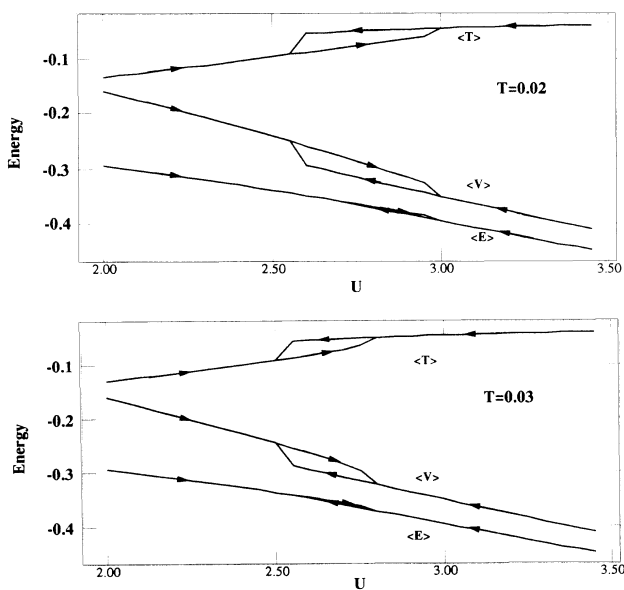

FIG. 9. The kinetic, potential, and internal energy as functions of U for (a) $T = 0.02$ and (b) $T = 0.03$. The hysteresis effect is clearly observed.
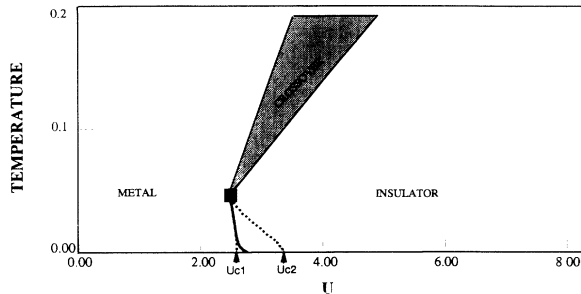

FIG. 10. Phase diagram of the fully frustrated Hubbard model at half filling. It is possible to move continuously from one phase to the other since at high T the transition becomes a crossover. The solid line is obtained by comparing the free energies of the two solutions in the region where they are both allowed. The dashed lines indicate the region where the metallic and the insulating solutions coexist. The filled square indicates the end of the first-order line in a second-order point.

We now turn to the determination of the Néel phase boundary. It depends on the nature of the lattice. For the Bethe lattice we solve Eqs. (6) and (7), while for the TSFFM introduced before, which mimics a finite degree of frustration, we solve Eqs. (8) and (9). The QMC method is used to estimate the magnetic phase boundary by solving the equations in the low-temperature region and determining the temperature where the staggered magnetization vanishes. The Néel temperature can be analytically determined on the insulating side for large U, and is given by $J_2 - J_1 = 2(t_2^2 - t_1^2)/U$. We mention in passing that the perturbative calculation does not correctly capture the magnetically ordered phase (see discussion in Sec. VI).

Figure 11 shows the phase boundary between paramagnetic states and antiferromagnetic states on the Bethe lattice. In this case, all the low-temperature features of the phase diagram discussed above are preempted by the onset of the antiferromagnetic state. On the other hand, for the case of the two-sublattice fully frustrated model, with values of $t_1^2 = \frac{1}{4}t^2$ and $t_2^2 = \frac{3}{4}t^2$, the Néel tempera-
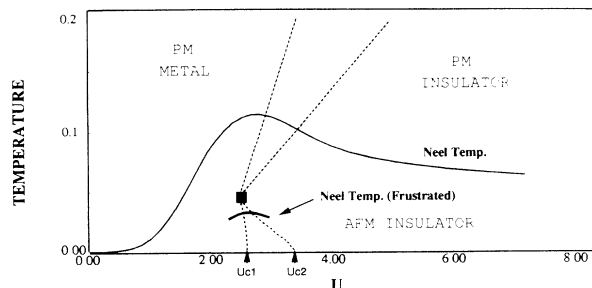

FIG. 11. Thin line corresponds the Néel temperature of the regular Bethe lattice as a function of interaction U. The bold line denotes an upper bound for the same quantity for the two-sublattice fully frustrated model with values $t_1^2 = 0.25t^2$, $t_2^2 = 0.75t^2$. The dotted lines are displayed for comparison to Fig. 10.

ture is much reduced. An upper bound for the $T_{\text{Néel}}$ as obtained from QMC simulations is indicated in Fig. 11. Simulations also indicate a jump in the Néel temperature line as the interaction U crosses the first-order transition boundary. The $T_{\text{Néel}}$ on the metallic side is smaller than the one on the insulating side.

It is clear that Slater's point of view is completely correct for nonfrustrated lattices such as the Bethe lattice with nearest-neighbor hopping only. The onset of antiferromagnetism makes the metal-insulator transition within the paramagnetic phase completely irrelevant. On the other hand, it is also clear that the presence of magnetic frustration makes Mott's viewpoint fully relevant, as demonstrated in the above diagram of the two-sublattice fully frustrated model.

IV. THE BREAKDOWN OF THE METALLIC SOLUTION

In this section we investigate the fate of the metallic solution. While we cannot settle the domain of stability of the metallic solution at zero temperature with the present approach, it is quite clear that the metal and the insulator are very close in energy and therefore the investigation of the metallic phase is of interest in the light of the considerably large mass renormalizations observed in some transition-metal oxides.

The destruction of the metallic state is driven by the collapse of the Fermi energy scale Δ which we showed is proportional to $U_{c2} - U$. From the mean-field equation $G_0^{-1} = i\omega_n - t^2 G$, we realize that this scale is also the *bandwidth* of the conduction-electron bath which hybridizes with the local impurity in the Anderson model picture. It is easy to understand, then, that for sufficiently large U this scale vanishes. Imagine solving the system of Eqs. (1), (2), and (3) by iteration. Consider a conduction-electron bandwidth Δ^n (W^n in the notation of Ref. 12) at the nth iteration step. For large U, solving the Kondo problem produces a bandwidth $\Delta^{n+1} = e^{-U/t}\Delta^n$. Therefore, the effective energy scale iterates to zero for $n \to \infty$.

Close to U_{c2}, there is a clear separation of energy scales and the local Green's function can be written as a sum of a low-energy and a high-energy part: G_l and G_h. The high-energy part resembles the solution of an atomic problem while the low-energy part obeys a scaling form. In terms of a spectral representation:

$$G_l = \int_{-\infty}^{\infty} \frac{\rho_l(\epsilon)}{i\omega-\epsilon} d\epsilon \tag{16}$$

$$G_h = \int_{-\infty}^{\infty} \frac{\rho_h(\epsilon)}{i\omega-\epsilon} d\epsilon, \tag{17}$$

with $\rho_l(\epsilon) = \frac{1}{t}f(\frac{\epsilon}{\Delta})$ exhibiting a scaling form as $\Delta \propto U_{c2} - U$ goes to zero. $\rho_h(\epsilon)$ describes the high-energy non-scaling parts (Hubbard bands) centered around $\pm U/2$. A somewhat oversimplified but transparent picture of the spectral function is obtained by taking ρ_h to be two semicircles with overall weight $1 - \Delta/D$, $t = D/2$. The calculation of the scaling function f is an open problem, in the exact solution of the large-d Hubbard model. Here we determine it within the second-order perturbation theory scheme outlined in Sec. II.

Approaching the transition, G_0 develops a pole at a scale $\sqrt{\Delta t} \gg \Delta$. The pole can be determined exactly from the relation $G_0^{-1} = i\omega - t^2 G$. In the frequency range of $\Delta \ll \omega \ll U/2$, the Green's function can be simplified to

$$G = \frac{2}{\omega}\int_0^\infty \rho_l(\epsilon)d\epsilon - 2\omega\int_0^\infty \frac{\rho_h(\epsilon)}{\epsilon^2}d\epsilon + i\pi\rho(\omega), \tag{18}$$

where particle-hole symmetry $\rho(-\epsilon) = \rho(\epsilon)$ has been used to change the integration limit. In the energy region we are considering, the imaginary part is negligibly small and we will ignore it in the following calculations.

$$G_0^{-1} = (1 + 2t^2 C)\omega - \frac{2t^2 \Delta F}{\omega}, \tag{19}$$

where $F = \frac{1}{t}\int_0^\infty f(x)dx$ and $C = \int_0^\infty \frac{\rho_h(\epsilon)}{\epsilon^2}d\epsilon$. The pole results at $\omega_0 = \sqrt{\Delta}(\frac{2t^2 F}{1+2t^2 C})^{1/2}$.

Notice that the existence of this pole follows from the general scaling argument. Now, combining this with the second-order expression for the self-energy, one can make further progress and determine the value of U_{c2} analytically.

The self-energy is $\Sigma = -U^2 G_0^3(\tau)$, which can be conveniently expressed in terms of the density of states of the G_0,

$$\Sigma = -2\omega U^2 \int_0^\infty \int_0^\infty \int_0^\infty \frac{\rho_0(\epsilon_1)\rho_0(\epsilon_2)\rho_0(\epsilon_3)d\epsilon_1 d\epsilon_2 d\epsilon_3}{(\epsilon_1 + \epsilon_2 + \epsilon_3)^2 - \omega^2} \tag{20}$$

where $\rho_0(\omega) = -\frac{1}{\pi}\text{Im}G_0(\omega)$. As $\Delta \to 0$, ρ_0 develops a δ-like peak positioned at ω_0 with a weight of $\frac{1}{2(1+2t^2 C)}$. Therefore, the integrals can be performed in closed form,

$$\Sigma = -\frac{U^2 \omega}{4(1 + 2t^2 C)^3(9\omega_0^2 - \omega^2)}, \tag{21}$$

as $\Delta \to 0$.

Comparing this expression with the one given by its definition, $\Sigma = G_0^{-1} - G^{-1} = -\frac{D\omega}{\Delta}$, where only the most singular term at small ω is kept, at $U = U_{c2}$ (i.e., $\Delta = 0$), we have

$$U_{c2} = 3D(1 + D^2/U_{c2}^2), \tag{22}$$

where $D = 2t$, and the approximations $F \approx \frac{1}{2D}$ and $C \approx \frac{2}{U_{c2}^2}$ that follow from the parametrization discussed before are used. The value at which the metallic solution disappears is then $U_{c2} = 3.28D$ which is very close to the numerically determined value $U_{c2}^{\text{num}} = 3.37D$. From Eq. (21) it is clear that the scaling part of Σ is proportional to $\frac{\omega}{\Delta}$ and that the scaling function f in this approximation is a semicircle. Figures 12(a) and 12(b) contain the numerical solution for the density of states ρ_l and its scaling form f, as obtained from the second-order perturbation theory supplemented by the self-consistent condition near U_{c2}. They demonstrate that the region where scaling holds is actually quite large.

In principle, Eq. (20) can be expanded to next order in Δ, but the coefficient depends on the scaling function and the high-energy part of the Green's function and cannot be calculated analytically. However, it can be determined numerically that, close to the critical point, $\Delta = k(U_{c2} - U)$ with $k = 0.23$. Recalling the definition of $\Delta = zD$ and that $\frac{m^*}{m} = z^{-1}$, this last result implies that within this approximation we find the same critical behavior for the divergence of the renormalized mass as in the work of Brinkman and Rice.[3] Notice that within second-order perturbation theory $\frac{\partial^2 \Sigma}{\partial \omega^2}$ is not divergent as one would expect on general grounds. This is due

to the fact that in this approach the vertex U is not renormalized.

V. THE BREAKDOWN OF THE INSULATING SOLUTION

In this section we study how the insulating solution disappears as we reduce the value of U. Our calculations determined that there indeed exists a new boundary $U_{c1}(T) < U_{c2}(T)$, $U_{c1}(T = 0) \approx 2.6D$ associated with the breakdown of the insulating solution.[22]

To understand the destruction of the insulating state, we again proceed to parametrize the Green's function.

$$G_0(\tau) = \alpha[\theta(\tau) - 1/2] + G_0^{\text{inc}}(\tau), \qquad (23)$$

the first term with $\theta(\tau)$ being the step function, represents an insulating solution at the atomic limit (t=0). G_0^{inc} is the "incoherent part" of the insulating solution, which decays to zero as $\tau \to \infty$ at zero temperature. Physically, this decomposition is motivated by viewing the self-consistent equations as describing a Kondo spin in an insulator. The spin operator S has a low-energy part which is responsible for a Curie type of local spin susceptibility and a high-frequency part. We write $S = \sqrt{\alpha} S_{\text{low}} + S_{\text{high}}$, where α is a quantity similar to the quasiparticle weight, describing the weight of a pure free spin in an interacting system, the impurity plus the insulating host. In frequency space, G_0^{inc} is only responsible for the details of the shape of the Hubbard bands which are high-frequency features. The step-function part gives rise to a divergency in $G_0(i\omega_n) \sim 1/i\omega_n$ and is solely responsible for the existence of a gap. In the atomic limit, α approaches unity, while on the contrary, the vanishing of α signals the complete screening (or Kondo quenching) of the spin and the destruction of the insulating phase.

Using the parametrized form of G_0, we can relate α to the density of states $\rho(\epsilon)$ of the local Green's function. At half filling, because of the particle-hole symmetry,

$$G = 2i\omega_n \int_0^\infty \frac{\rho(\epsilon)d\epsilon}{(i\omega_n)^2 - \epsilon^2}. \qquad (24)$$

Therefore, using (3) and comparing linear terms in $i\omega$,

$$\alpha^{-1} = 1 + 2t^2 \int_0^\infty \frac{\rho(\epsilon)d\epsilon}{\epsilon^2}. \qquad (25)$$

If the Mott-Hubbard gap collapses, i.e., $\rho(\epsilon)$ becomes finite at $\epsilon \to 0$, α^{-1} diverges. Alternatively, a finite α at the transition indicates a finite Mott-Hubbard gap. Within the second-order perturbation scheme, we can obtain a closed equation for α. Inserting the parametrized G_0 into the self-energy expression we obtain

$$\Sigma(\tau) = \alpha^3 \left(\frac{U}{2}\right)^2 [\theta(\tau) - 1/2] + \Sigma_{\text{inc}}, \qquad (26)$$

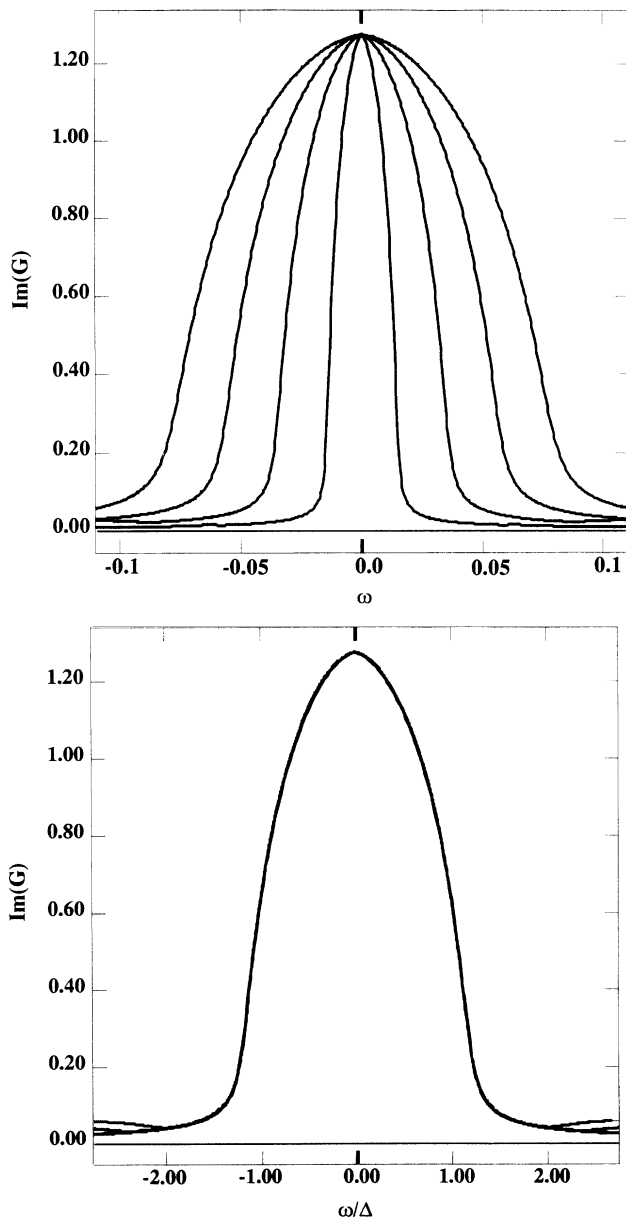which determines the low-frequency behavior of the local Green's function:

FIG. 12. (a) Low-frequency part of the density of states $\rho(\omega)$ as function of the frequency for values of the interaction $U = 3, 3.1, 3.2, 3.3$. (b) The four curves of (a) collapse to one universal form after rescaling: $f(\frac{\omega}{\Delta}) = t\rho_l(\omega)$, where $\Delta \propto U_c - U$.

$$G = \frac{2}{\{i\omega_n + \Sigma(G_0) + i\mathrm{sgn}(\omega_n)\sqrt{D^2 + [\omega_n + i\Sigma(G_0)]^2}\}}. \tag{27}$$

Considering the most singular terms in the self-consistency condition in Eqs. (2) and (3), for small ω we have

$$G_0^{-1} = i\omega_n + \frac{D^2}{4\Sigma}, \tag{28}$$

and therefore,

$$\alpha = \left(1 + \frac{D^2}{U^2\alpha^3}\right)^{-1}. \tag{29}$$

There are two solutions for α^* for $U > U_{c1}$. The one with a smaller α^* is always unstable and unphysical since it is not connected continuously to $\alpha = 1$ as U tends to infinity. At the transition U_{c1}, the unstable fixed point collides with the stable one, and the fixed-point solution disappears. $U_{c1} = 3\sqrt{3}/2D \approx 2.6D$ which is the same as the result numerically obtained. Since α is finite at the transition, the Mott-Hubbard gap is finite. Across the critical line $U_{c1}(T)$ there is a first-order jump in the dielectric constant. There are, however, soft fluctuations associated with fluctuations in α . An important issue left open is whether α diverges as $U \to U_{c1}$ in the full solution. As was previously noted in Sec. II, we observed using QMC that in the exact finite-temperature solution the U_{c1} vs T line is shifted to lower values of U, indicating a further reduction of the minimum gap. We are not able to determine whether the gap collapses to zero as in Hubbard's original scheme ($\alpha \propto U - U_{c1}$), or whether it remines finite until it disappears, as described by the second-order perturbation scheme.

VI. SUSCEPTIBILITIES AND THE MOTT-HUBBARD TRANSITION

In what follows we are going to present a combination of theoretical arguments and numerical results, in order to discuss the behavior of the susceptibilities in the vicinity of the transition. Unfortunately, we cannot take further advantage of the perturbative approach. The vanishing of higher-order corrections in the self-energy in the atomic limit does not necessarily imply that this will be true also for the calculation of other quantities. Therefore, all the numerical results in this section were obtained with the QMC method. Although the present computational power does not allow a detailed quantitative analysis of higher correlation functions at very low temperatures, our results are sufficient to give support to the theoretical discussion.

Much theoretical insight about the behavior of the spin and charge susceptibilities can be gained from the fact that the impurity model describing the Hubbard model is an Anderson impurity model.

In a previous work we have already discussed the fact that, when the Mott point is approached, magnetic order of the local spin sets in.[13] This is observed from the

plots of the imaginary-time spin-spin correlation function which exhibit a divergence in $\chi_L^s = \int_0^\beta \langle m_z(\tau)m_z(0)\rangle d\tau$, shown in Fig. 13.

In principle χ_L^s can be determined in NMR experiments. However, it is the $q = 0$ susceptibility that is easily accessible to experimental probes. The $q = 0$ quantities differ from the local ones because of the polarization of the Weiss field due to the external perturbation. We will illustrate how this effect, which is at the heart of Fermi liquid theory, modifies the low-energy responses near U_{c2}.

In the presence of a small chemical potential away from the particle-hole symmetric value and a small magnetic field, the mean-field equations are

$$G_{0\sigma}^{-1} = i\omega_n + \mu + \sigma h - t^2 G_\sigma. \tag{30}$$

To proceed, we extend the simplified form of the parametrization discussed in Sec. IV to account for the magnetic properties. The high-frequency part of the Green's function is polarized like a local moment which can be described as a superposition of Hartree-Fock solutions. It has been demonstrated that as $U \sim U_c$ the upper and lower Hubbard bands are well developed, so that for low frequencies and fields, a good approximation for G_σ is

$$G_\sigma = \frac{n_\sigma}{[i\omega_n - \frac{U}{2}]} + \frac{n_{-\sigma}}{(i\omega_n + \frac{U}{2})} + \frac{2}{D}\frac{\Delta}{i\omega_n + \Delta(\mathrm{sgn}\omega_n)}. \tag{31}$$

Inserting (31) in (30), we have for small frequencies,

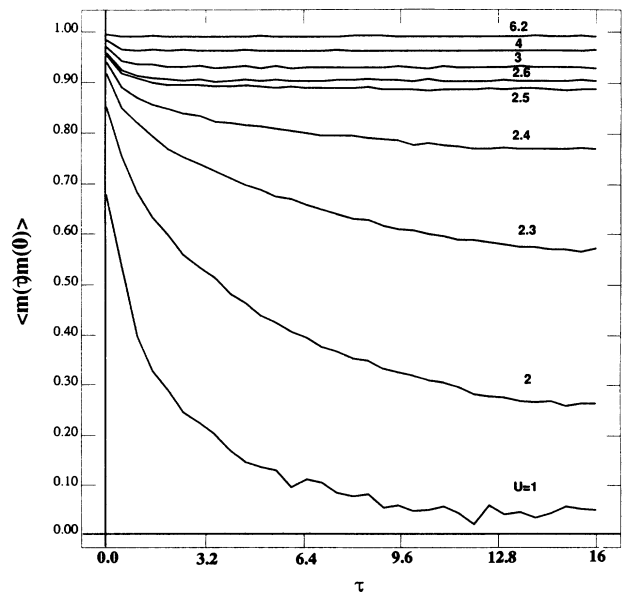$$G_{0\sigma}^{-1} = i\omega_n + \mu + h\sigma + 2\frac{t^2 m_\sigma}{U} \tag{32}$$

FIG. 13. Moment-moment correlation function as a function of imaginary time at $\beta = 32$. (See Ref. 28.)

where $n_\sigma = n + \frac{m_\sigma}{2}$. Equation (32) describes an impurity problem in the presence of an external field $h_{\rm eff} = h - 2\frac{t^2}{U}m_\sigma$. We can compute the magnetization from the theory of the Anderson impurity model in an effective field $h_{\rm eff}$. We know that $m = \chi_0 h_{\rm eff}$ with $\chi_0 \sim \frac{1}{\alpha T_k}$, where T_k is the effective Kondo energy of the problem, which in our case corresponds to Δ, and α is a numerical coefficient of order unity. Solving for m we find

$$\chi_s = \left[\frac{dm}{dh}\right]_{h=0} = \frac{1}{[\chi_0^{-1} + 2\frac{t^2}{U}]} = \frac{1}{\alpha\Delta + J_0} \qquad (33)$$

where we have defined the magnetic exchange energy $J_0 = 2\frac{t^2}{U}(= \frac{D^2}{2U})$.

The physical interpretation of this equation is transparent: the exchange arises from high-energy processes which are largely unaffected by the Mott transition. As a result the susceptibility varies continuously, as U passes through U_c. Remarkably, Eq. (33) was also obtained in the large-N limit.[23] These findings are consistent with the QMC results of Fig. 14. For smaller U, an initial fast increase in χ_s is observed as Δ rapidly decreases. As the critical value of U is approached we see the divergency being cut off by the finite magnetic exchange J_0.

Similar considerations apply to the charge susceptibility. Applying a chemical potential does not cause a change (to order δn) in the distribution of integrated spectral weight between the upper and lower Hubbard bands. This can be readily understood by extending the observation of Ref. 12 that the high-energy features are correctly reproduced by an expansion around the atomic limit. In this limit a small particle-hole asymmetry shifts the energies of the atomic levels but does not transfer spectral weight. The change in the low-energy part of the Green's function is easily estimated using Fermi liquid theorems. The change in $G(0)$ as a result of a change in chemical potential is given by the phase shift, which

in turn is given by the shift of the location of the center of the resonance. Its width does not change to order Δ because of particle-hole symmetry. Assuming that at low frequencies the result of applying μ is to shift the center of the resonance by ϵ_f:

$$G(i\omega_n) \simeq \frac{\Delta}{(i\omega_r + \epsilon_f + i\Delta{\rm sgn}\omega_n)} \qquad (34)$$

with $\delta n \simeq \frac{\epsilon_f}{\pi\Delta}$. We find $\delta G(0) = \frac{\delta n}{\Delta}$ and, therefore, from Eq. (30), the effective chemical potential seen in the impurity model is $\delta\mu_{\rm eff} = \delta\mu - \frac{t^2}{\Delta}\delta n$. The response of the impurity to this shift in the chemical potential is $\delta n = \chi_{\rm imp}\delta\mu_{\rm eff}$, with $\chi_{\rm imp} \simeq \frac{1}{U}$ the charge susceptibility of the impurity. Combining these equations we obtain:

$$\frac{\delta n}{\delta\mu} = \frac{\chi_c^0}{\left(1 + \frac{\chi_c^0 t^2}{\Delta}\right)} \simeq \Delta, \qquad (35)$$

that is, the charge susceptibility vanishes as $(U_c - U)$ as we approach the Mott transition. These results are also consistent with the numerical simulations. Figure 15 shows the slope of the μ vs n curves going to zero as U approaches U_c. On the other hand, the moment $\langle(n_\uparrow - n_\downarrow)^2\rangle$, a quantity closely related to the double occupancy, does not saturate as the transition is crossed, as can be seen in Fig. 16. This is consistent with the local charge susceptibility being finite. In fact, the impurity charge compressibility equals minus the kinetic energy by virtue of the mean-field equations.

We argued before that the local spin susceptibility diverges at the Mott transition as $\frac{1}{\Delta}$ while the $q = 0$ spin susceptibility stays finite at the transition. This and an independent estimate of the exchange constant J_0 can be obtained by approaching the transition from the insulat-
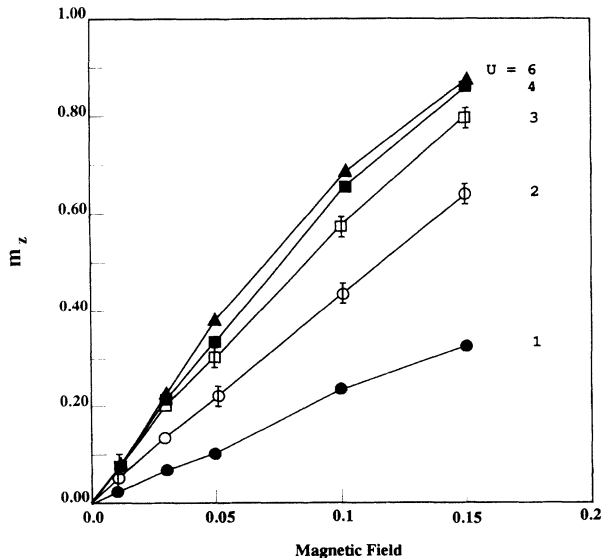

FIG. 14.   Local magnetization m_z as function of an external magnetic field, for different values of the interaction U.
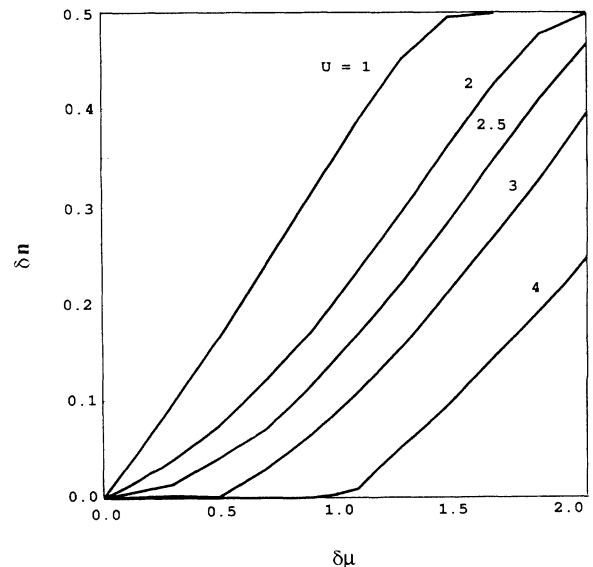

FIG. 15.   Difference in the occupation number δn from the half-filled case as a function of the chemical potential $\delta\mu = \mu - U/2$, for different values of the interaction U.
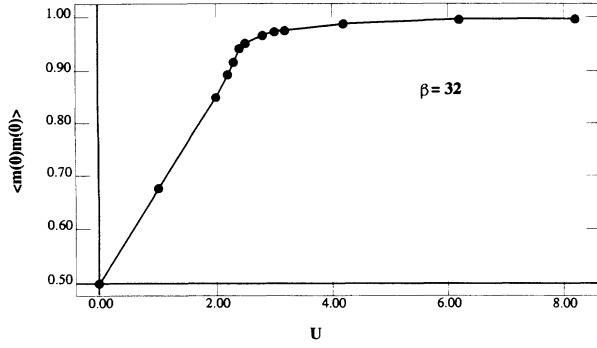
FIG. 16. Local magnetic-moment formation $\langle m_z^2 \rangle$ as a function of interaction U for inverse temperature $\beta = 32$. The double occupancy $\langle D \rangle$ can be simply obtained from $\langle m_z^2 \rangle = 1 - 2\langle D \rangle$. (See Ref. 28.)

ing side and by analyzing the fully frustrated model.

For large U, the fully frustrated model in Eq. (4) reduces at half filling to

$$H_J = \sum_{ij} J_{ij} S_i \cdot S_j, \tag{36}$$

where J_{ij} are independent random variables with an exponential distribution $P\{J\} = \frac{\Theta(J)}{\sqrt{J}}\exp - (JN/J_0)$, with $\theta(x) = 1$ for $x > 0$ and $\theta(x) = 0$ for $x < 0$.

An important observation is that $\bar{J}_{ij} = \frac{J}{N}$ while the variance $\bar{J}_{ij}^2 - \bar{J}_{ij}^2 = \frac{J^2}{N^2}$ so the randomness is irrelevant in the thermodynamical limit. The solution of Hamiltonian (36) with $J_{ij} = \frac{J}{N}$ is elementary.

We exhibit the solution to confirm and interpret the finite susceptibility in the insulating phase. The eigenstates of Eq. (36) are labeled by the total spin $\epsilon_s = \frac{J_0}{N}[S(S + 1)]$. For simplicity we will take N to be even, $N \equiv 2N_0$. For a given value of the spin the degeneracy of a state with a given value of total spin S and projection S_Z is: $d_S = \binom{2N_0}{N_0-S} - \binom{2N_0}{N_0-S-1}$. The partition function in the presence of a uniform field reduces to:

$$Z = \sum_{S=0}^{N_0} d_S e^{-\beta \frac{J_0}{2N_0} S(S+1)} \frac{\sinh[\beta h(S + \frac{1}{2})]}{\sinh(\frac{\beta h}{2})}. \tag{37}$$

In the thermodynamical limit $N_0 \to \infty$ it is convenient to introduce the variable $x = S/N_0$ and Eq. (37) reduces to

$$Z = N_0 \left\{ \int_0^1 dx e^{N_0 g(x)} e^{-\frac{\beta J_0 N_0 x^2}{4}} \right.$$
$$\left. \times \left[\frac{e^{h\beta N_0 x} - e^{-h\beta N_0 x}}{2\sinh(\frac{h\beta}{2})} \right] + O\left(\frac{1}{N_0}\right) \right\} \tag{38}$$

with $g(x) \equiv \ln\frac{4}{(1+x)(1-x)} + x\ln[\frac{1-x}{1+x}]$ being the density of states. This system is peculiar in that the number of states decreases as the energy (or the spin) increases. $g(x) = 2\ln2 - x^2$ as $x \to 0$, and therefore it has negative temperature. Equation (38) is easily evaluated when N_0

is large, and we obtain the free energy per particle

$$\frac{F(h, \beta)}{N} = -\frac{h^2 \beta}{(8 + 2\beta J_0)} - \frac{1}{\beta}\ln2, \tag{39}$$

and the susceptibility

$$\chi^s(q = 0) = -\frac{\partial^2 f}{\partial h^2} = \frac{1}{(4T + J_0)}, \tag{40}$$

which displays the Curie law for $T \gg J_0$ but saturates at the magnetic energy J_0 at low temperatures, in complete agreement with the discussion of the paramagnetic phase. From the free energy we can extract the entropy and the energy $-E = \frac{\partial \ln Z}{\partial \beta}$ and $S = \frac{E-F}{T}$. Notice that when $h = 0, E = 0$ and $S = 2N_0\ln2$. This is the result of the large degeneracy of the singlet sector. In fact the number of states per particle in the singlet sector can be estimated directly from Eq. (39).

The prediction that χ^s remains finite as $U \to U_{c2}$ is physically sensible and probably persists in finite dimensions. It reflects the fact that the magnetic energy is finite when $d \to \infty$. The same is true in the limit of large N of the model studied in Ref. 24 in any dimension, provided we identify the Mott transition with the metal–charge-transfer-insulator transition. This physics is missed by the Gutzwiller approximation, which ignores the high-energy processes and thus the magnetic exchange completely. The divergence of γ (cf. Sec. III) as $U \to U_c$ is consistent with the fact that the entropy is ln2 in the insulator. In the metallic phases $S(T) = \int_0^T \frac{C_v(T')}{T'}dT'$. Since this quantity vanishes as $T \to 0$ in the insulating phase $\frac{C_v(T)}{T}$ diverges at the transition. This is the result of a large spin ground-state degeneracy. It is rooted in the fact that since $J_{ij} \sim \frac{1}{d}$ one needs long-range order to gain finite magnetic energy. This is clearly unrealistic and will not persist in any finite dimension. In fact, in the large-N limit in finite dimensions the specific heat remains finite when the metal-insulator transition drives the system into a resonating-valence-bond state.[25] It would be interesting to construct a loop expansion around the $d = \infty$ solution to remedy this problem.

We also demonstrated that for $U < U_{c2}$, the one-particle Green's function of the model captures some aspects of the Brinkman-Rice scenario. In particular, the mass renormalization diverges as $(U_{c2} - U)^{-1}$.[13] At the same time the solution of the Hubbard model in infinite dimension also allowed us to perform calculations of physical quantities at finite temperatures and eliminate some of the shortcomings of the Brinkman-Rice description of the Mott transition. In the actual solution, the number of doubly occupied sites is finite and changes smoothly at the metal-insulator transition[15,13] resulting in a finite exchange constant which gives rise to a finite susceptibility. We also observed that the single-particle gap opens discontinuously at U_{c2}, which is different from the predictions of the slave-boson method,[23] but is not inconsistent with the experimental observations of Fujimori et al.[26]

VII. COMPARISON WITH EXPERIMENTS

A theory of the Mott transition would be incomplete without a comparison to some of the existing experiments on the subject. Our goal here is to assess to what extent the Hubbard model in the limit of large dimensions capture the main trends of transition-metal oxides near the Mott transition, rather than to obtain the best possible fit to the experimental data.

We first focus on the beautiful set of experiments by the group of Tokura et al., where the system $La_{1-x}Sr_xTiO_3$ is studied as a function of doping x.[19] They measured the specific heat coefficient γ as a function of x. Since the photoemission study shows that the $x = 0$ point is close to the Mott transition,[26] we picked $U = 3.2D$ and performed quantum Monte Carlo simulation to calculate γ vs doping. The results are shown in Fig. 17, together with the experimental data. The agreement is quite good.

We finally turn to the V_2O_3 system. This system was studied extensively before, and has been studied again most recently by Carter et al.[18] We have compared the experimental phase diagram with the one obtained for the two-sublattice fully frustrated model. On a qualitative level we find that the overall agreement is remarkably good, especially regarding the features of the three phase boundaries, antiferromagnetic insulator to paramagnetic metal, paramagnetic metal to paramagnetic insulator, paramagnetic insulator to antiferromagnetic insulator, and the crossover regime. Interestingly, we also found a small region of a metallic antiferromagnetic state similar to the experimental observation of Ref. 18. Unfortunately, it occurs at a very low temperature and the

determination of the phase boundary is outside the applicability of the QMC method. Nevertheless the existence of this phase can be seen by a simple Hartree-Fock calculation in the frustrated case.

It is also notable that the temperature scales are consistent if an energy of $D = 1$ eV is considered. The comparison on the abscissa is less transparent. In this case, we have identified increasing pressure as increasing hopping constant t or decreasing interaction U.

VIII. CONCLUSION

The solution of the Hubbard model in the limit of large dimensions has provided a limit where various early ideas can be put in perspective.

One issue is whether a metal-insulator transition can take place in the absence of magnetic order. The phase diagram presented in Figs. 10 and 11 answers this question in the affirmative for a frustrated lattice. The phase diagram has the same topology and even the same scale as the experimentally observed phase diagram of V_2O_3.

There is a region enclosed by two lines $U_{c1}(T)$ and $U_{c2}(T)$, where both the metallic and the insulating solutions are allowed. Within this region, there is a first-order boundary where the two very different solutions cross in free energy, and several quantities experience a jump: the specific heat, the susceptibility, the number of doubly occupied sites, etc. The first-order line has a negative slope, indicating that the paramagnetic insulating phase has a higher entropy than the metallic phase. The line ends in an interesting second-order critical point, above which there is a smooth crossover between a metallic and an insulating regime. In the frustrated lattice, in addition, at low temperatures there is a first-order line between an antiferromagnetic metal and an antiferromagnetic insulating phase. We therefore conclude that the Hubbard model in large dimensions at half filling on a frustrated lattice can account for the basic experimentally observed features of the V_2O_3 system, vindicating Mott's point of view.

On nonfrustrated, bipartite lattices, however, we find that the Néel temperature is much higher than the metal-insulator transition temperature, making the transition between small and large U continuous. In this case the physics can be understood in terms of the magnetic long-range order and a smooth crossover within the broken-symmetry phase. The Mott transition is irrelevant, vindicating Slater's point of view.

Within the second-order perturbation scheme we establish that there is a metallic solution with a collapsing energy scale at U_{c2}, realizing the Brinkman-Rice scenario. We were unable to prove that this solution is stable down to U_{c2} because the energy differences between the metallic and insulating solutions are very small. However, assuming the stability of the solution we were able to calculate the critical behavior of various physical quantities and make contact with the recent experiments of Ref. 19. We conclude that the Hubbard model in large dimensions, therefore, supports the Brinkman-Rice scenario for the destruction of the metal and eliminates many of its shortcomings.
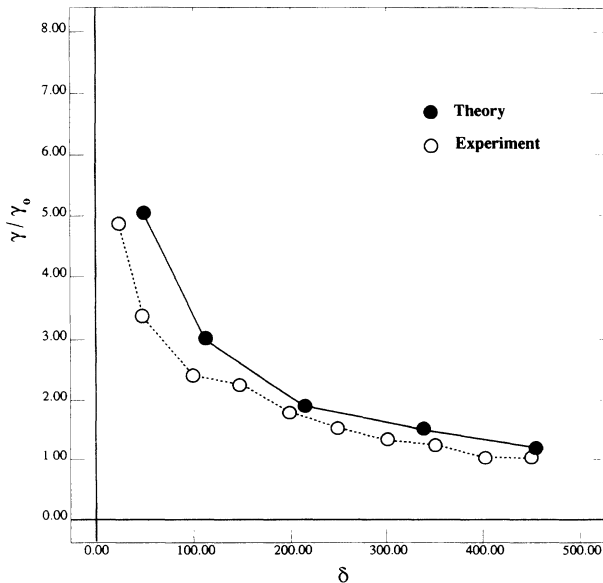

FIG. 17. Comparison to experimental observation of the linear coefficient of the specific heat γ as a function of doping for an inverse temperature of $\beta = 32$. Experimental results from Ref. 19. Quantities normalized to the full (or zero) filling value.

A natural scenario for the destruction of the insulating solution would be a continuous narrowing of the gap of the insulator. This would have been a realization of the original Hubbard scenario for the metal-insulator transition driven by the closing of the upper and lower Hubbard bands. In this case, U_{c1} would have corresponded to the value of the interaction where the gap in the one-particle spectra vanishes, or equivalently where the divergence of the dielectric constant is observed. This does not occur, at least within the second-order approximation to the impurity self-energy.

The experimentally observed phase diagrams of transition-metal oxides display incommensurate metallic magnetism. This can in principle be studied by extending the mean-field theory to account for incommensurate phases, as done by Freericks for the Falicov-Kimball model.[27] For this calculation to be meaningful, however, one should include the details of a realistic band structure of the transition-metal oxide, which is beyond the scope of our work.

An important open question is what happens to the transition at finite dimensions? We expect that the Mott transition and the metal–charge-transfer-insulator transition are in the same universality class. The large-N expansion results of Ref. 24 indicate that, for $N = 2$,

U_{c1} and U_{c2} coincide and that the Mott transition is second order with continuous disappearance of the Kondo resonance and a gradual closing of the Mott gap. Similar results were obtained with the slave-boson approach to the Hubbard model. Whether the large-N expansion is missing crucial $1/N$ terms which would split the two transitions, or whether the $1/d$ corrections would bring the two transitions to one, remains an interesting open problem.

Note added in proof. Recently, two zero-temperature algorithms based on exact diagonalization were developed.[29,30] We have confirmed that U_{c1} is strictly less than U_{c2} and shown that the MIT at $T = 0$ takes place at U_{c2}.[31]

ACKNOWLEDGMENT

[1] N. F. Mott, Philos. Mag. **6**, 287 (1961).

[2] J. Hubbard, Proc. R. Soc. (London) **A281**, 401 (1964).

[3] W. F. Brinkman and T. M. Rice, Phys. Rev. B **2**, 4302 (1970).

[4] J. C. Slater, Phys. Rev. **82**, 538 (1951).

[5] W. Metzner and D. Vollhardt, Phys. Rev. Lett. **62**, 324 (1989).

[6] U. Brandt and C. Mielsch, Z. Phys. **75**, 365 (1989); **79**, 295 (1990); **82**, 37 (1991).

[7] V. Janis, Z. Phys. B **83**, 227 (1991).

[8] E. Müller-Hartmann, Z. Phys. B **74**, 507 (1989); Z. Phys. B **76**, 211 (1989).

[9] A. Georges and G. Kotliar, Phys. Rev. B **45**, 6479 (1992).

[10] V. Janis and D. Vollhardt, Int. J. Mod. Phys. B **6**, 731 (1992).

[11] A. Georges, G. Kotliar, and Q. Si, in *Proceedings of the Trieste Meeting on Strongly Correlated Electron Systems* [Int. J. Mod. Phys. B **6**, 705 (1992)].

[12] M. J. Rozenberg, X. Y. Zhang, and G. Kotliar, Phys. Rev. Lett. **69**, 1236 (1992).

[13] X. Y. Zhang, M. J. Rozenberg, and G. Kotliar, Phys. Rev. Lett. **70**, 1666 (1993).

[14] M. Jarrell, Phys. Rev. Lett. **69**, 168 (1992); Th. Pruschke, D. L. Cox, and M. Jarrell, Eur. Phys. Lett. **21**, 5 (1993); Phys. Rev. B. **47**, 3553 (1993).

[15] A. Georges and W. Krauth, Phys. Rev. Lett. **69**, 1240 (1992).

[16] A. Georges and W. Krauth Phys. Rev. B **48**, 7167 (1993).

[17] V. Janis, M. Ulmke, and D. Vollhardt (unpublished).

[18] S. A. Carter, T. F. Rosenbaum, J. M. Honig, and J. Spalek, Phys. Rev. Lett. **67**, 3440 (1992).

[19] Y. Tokura, Y. Taguchi, Y. Okada, Y. Fujishima, T. Arima, K. Kumagai, and Y. Iye, Phys. Rev. Lett. **70**, 2126 (1993).

[20] A. Georges and S. Sachdev (unpublished).

[21] K. Yamada, Prog. Theor. Phys. **53**, 970 (1975); K. Yosida and K. Yamada, *ibid.* **53**, 1286 (1975).

[22] This possibility was suggested to us by D. Fisher as a way of reconciling the numerical results of our group and those of the ENS group.

[23] G. Kotliar, Int. J. Mod. Phys. B **1**, 711 (1988).

[24] C. Castellani, G. Kotliar, R. Raimondi, M. Grilli, Z. Wang, and M. Rozenberg, Phys. Rev. Lett. **68**, 2009 (1992).

[25] M. Grilli and G. Kotliar, Phys. Rev. Lett. **64**, 1170 (1990).

[26] A. Fujimori, I. Hase, H. Namatame, Y. Fujishima, Y. Tokura, H. Eisaki, S. Uchida, K. Takegahara, and F. M. F. de Groot, Phys. Rev. Lett. **69**, 1796 (1992).

[27] J. Freericks (unpublished).

[28] Figures 13 and 16 contain small corrections to the corresponding figures of Ref. 13.

[29] Q. Si, M. J. Rozenberg, G. Kotliar, and A. Ruckenstein (unpublished).

[30] M. Caffarel and W. Krauth (unpublished).

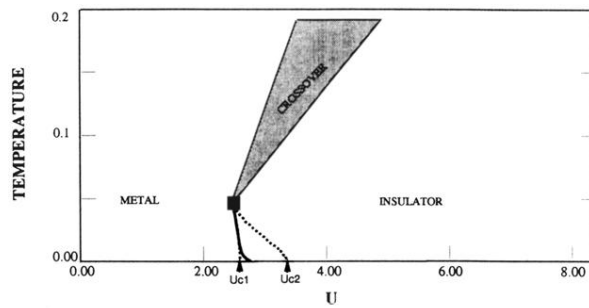[31] M. J. Rozenberg, G. Moeller, and G. Kotliar (unpublished).

FIG. 10. Phase diagram of the fully frustrated Hubbard model at half filling. It is possible to move continuously from one phase to the other since at high T the transition becomes a crossover. The solid line is obtained by comparing the free energies of the two solutions in the region where they are both allowed. The dashed lines indicate the region where the metallic and the insulating solutions coexist. The filled square indicates the end of the first-order line in a second-order point.